Feedback between p21 and reactive oxygen production is necessary for cell senescence

João F Passos[1,2], Glyn Nelson[1,2], Chunfang Wang[1,2], Torsten Richter[1], Cedric Simillion[2], Carole J Proctor[1,2], Satomi Miwa[1,2], Sharon Olijslagers[1], Jennifer Hallinan[2], Anil Wipat[2], Gabriele Saretzki[2,3], Karl Lenhard Rudolph[4], Tom BL Kirkwood[1,2] and Thomas von Zglinicki[1,2,*]

[1] Ageing Research Laboratories, Institute for Ageing and Health, Newcastle University, Newcastle upon Tyne, UK, [2] Centre for Integrated Systems Biology of Ageing and Nutrition, Institute for Ageing and Health, Newcastle University, Newcastle upon Tyne, UK, [3] Crucible Laboratory, Institute for Ageing and Health, Newcastle University, Newcastle upon Tyne, UK and [4] Department of Molecular Medicine and Max-Planck Research Group on Stem Cell Aging, University of Ulm, Ulm, Germany
* Corresponding author. Institute for Ageing and Health, Campus for Ageing and Vitality, Newcastle University, Newcastle upon Tyne NE4 5PL, UK.
Tel.: +44 191 248 1104; Fax: +44 191 248 1101; E-mail t.vonzglinicki@ncl.ac.uk

Cellular senescence—the permanent arrest of cycling in normally proliferating cells such as fibroblasts—contributes both to age-related loss of mammalian tissue homeostasis and acts as a tumour suppressor mechanism. The pathways leading to establishment of senescence are proving to be more complex than was previously envisaged. Combining *in-silico* interactome analysis and functional target gene inhibition, stochastic modelling and live cell microscopy, we show here that there exists a dynamic feedback loop that is triggered by a DNA damage response (DDR) and, which after a delay of several days, locks the cell into an actively maintained state of 'deep' cellular senescence. The essential feature of the loop is that long-term activation of the checkpoint gene CDKN1A (p21) induces mitochondrial dysfunction and production of reactive oxygen species (ROS) through serial signalling through GADD45-MAPK14(p38MAPK)-GRB2-TGFBR2-TGFβ. These ROS in turn replenish short-lived DNA damage foci and maintain an ongoing DDR. We show that this loop is both necessary and sufficient for the stability of growth arrest during the establishment of the senescent phenotype.
Molecular Systems Biology **6**: 347; published online 16 February 2010; doi:10.1038/msb.2010.5
Subject Categories: metabolic and regulatory networks; differentiation and death
Keywords: aging; cell senescence; DNA damage foci; mitochondria; reactive oxygen

Introduction

Cellular senescence is defined by the irreversible loss of division potential of somatic cells and a variety of associated phenotypic changes (Campisi and d'Adda di Fagagna, 2007). Recent interest has been spurred by mounting evidence for major roles for cellular senescence *in vivo*: on the one hand, oncogene-triggered senescence is a potentially very powerful tumour suppression mechanism (Ramsey and Sharpless, 2006; Bartek *et al*, 2007). On the other hand, cellular senescence might contribute to the loss of tissue homeostasis in mammalian aging. There is evidence that senescence-marker-positive cells increase with age in various tissues (Dimri *et al*, 1995; Krishnamurthy *et al*, 2004; Herbig *et al*, 2006; Wang *et al*, 2009) and in age-related diseases including atherosclerosis (Minamino and Komuro, 2007) and diabetes (Sone and Kagawa, 2005). Although it is not known for how long senescent cells persist *in vivo* (Ventura *et al*, 2007; Krizhanovsky *et al*, 2008), there is a clear evidence that senescent check point

activation can contribute to organismal aging (Rudolph *et al*, 1999; Tyner *et al*, 2002; Choudhury *et al*, 2007).

A DNA damage response (DDR), triggered by uncapped telomeres or non-telomeric DNA damage, is the most prominent initiator of senescence (d'Adda di Fagagna, 2008). This response is characterized by activation of sensor kinases (ATM/ATR, DNA-PK), formation of DNA damage foci containing activated H2A.X (γH2A.X) and ultimately induction of cell cycle arrest through activation of checkpoint proteins, notably p53 (TP53) and the CDK inhibitor p21 (CDKN1A). This signalling pathway continues to contribute actively to the stability of the G0 arrest in fully senescent cells long after induction of senescence (d'Adda di Fagagna *et al*, 2003). However, interruption of this pathway is no longer sufficient to rescue growth once the cells have progressed towards an established senescent phenotype (d'Adda di Fagagna *et al*, 2003; Sang *et al*, 2008).

Senescence is clearly more complex than CDKI-mediated growth arrest: senescent cells express hundreds of genes

differentially (Shelton *et al*, 1999), prominent among these being pro-inflammatory secretory genes (Coppe *et al*, 2008) and marker genes for a retrograde response induced by mitochondrial dysfunction (Passos *et al*, 2007a). Recent studies showed that activated chemokine receptor CXCR2 (Acosta *et al*, 2008), insulin-like growth factor binding protein 7 (Wajapeyee *et al*, 2008), IL6 receptor (Kuilman *et al*, 2008) or downregulation of the transcriptional repressor HES1 (Sang *et al*, 2008) may be required for the establishment and/or maintenance of the senescent phenotype in various cell types. A signature pro-inflammatory secretory phenotype takes 7–10 days to develop under DDR (Coppe *et al*, 2008; Rodier *et al*, 2009). Together, these data suggest that senescence develops quite slowly from an initiation stage (e.g. DDR-mediated cell cycle arrest) towards fully irreversible, phenotypically complete senescence. It is the intermediary step(s) that define the establishment of senescence, which are largely unknown with respect to kinetics and governing mechanisms.

Reactive oxygen species (ROS) are likely to be involved in establishment and stabilization of senescence: elevated ROS levels are associated with both replicative (telomere-dependent) and stress- or oncogene-induced senescence (Saretzki *et al*, 2003; Ramsey and Sharpless, 2006; Passos *et al*, 2007a; Lu and Finkel, 2008). ROS accelerate telomere shortening (von Zglinicki, 2002) and can damage DNA directly and thus induce DDR and senescence (Chen *et al*, 1995; Lu and Finkel, 2008; Rai *et al*, 2008). Conversely, activation of the major downstream effectors of the DDR/senescence checkpoint can induce ROS production (Polyak *et al*, 1997; Macip *et al*, 2002, 2003). Thus, cause–effect relationships between cellular ROS production and senescence are not sufficiently clear.

Here, we analyse the role of ROS for the establishment of senescence initiated by DNA damage or telomere dysfunction and show the existence of a positive feedback loop between DDR and ROS production. We show that telomere-dependent or -independent DDR triggers mitochondrial dysfunction leading to enhanced ROS activation through a linear signal transduction through TP53, CDKN1A, GADD45A, p38 (MAPK14), GRB2, TGFBR2 and TGFβ. ROS contribute in a stochastic manner to the long-term maintenance of DNA damage foci, and this is necessary and sufficient to maintain proliferation arrest in response to DNA damage during the establishment of an irreversible senescent phenotype. Our results provide experimental evidence that ROS-dependent signalling is required for the establishment of irreversible senescence of cells with dysfunctional telomeres or damaged DNA *in vitro* and *in vivo*. This result might be relevant for therapeutic studies aiming to modulate intracellular ROS levels in both aging and cancer.

Results

Delayed mitochondrial dysfunction and ROS production are a consequence of senescence
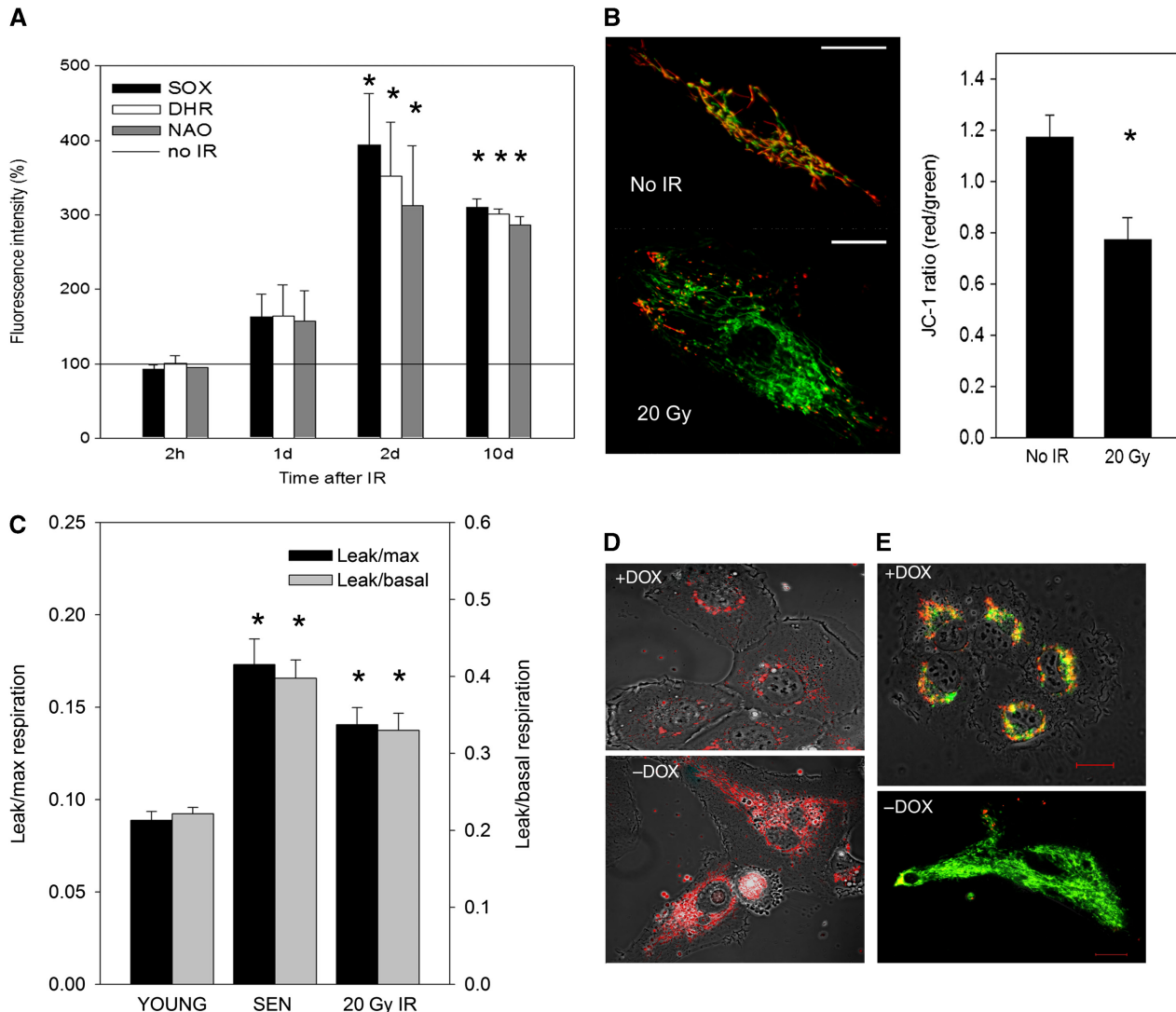
To measure the kinetics of ROS induction in senescence, we treated proliferation-competent human MRC5 fibroblasts with ionizing radiation (IR, 20 Gy). This abolished cell growth and labelling indices for BrdU, Ki67 and caused expression of senescence-associated β-galactosidase (Sen-β-Gal) to an extent equal to the deep replicative senescence seen when cells had reached their normal proliferative limit (data not shown; Supplementary Figures S1A and B). After IR, DNA damage foci frequencies remained permanently elevated (Supplementary Figures S1C–E) but did not co-localize with telomeres (Supplementary Figure S1F), together indicating that the cells were driven into stress-induced premature senescence (SIPS). Importantly, the levels of mitochondrial superoxide (measured as MitoSOX fluorescence intensity in flow cytometry) and cellular peroxides (dihydrorhodamine 123/DHR fluorescence intensity) did not alter immediately after IR but after 24 h the levels of both ROS indicators increased and remained elevated over the entire observation period from day 2 onwards (Figure 1A). This delayed change in ROS indicators was accompanied by a corresponding increase in mitochondrial mass measured by nonyl acridine orange (NAO) fluorescence (Figure 1A) and decreased mitochondrial membrane potential measured by JC-1 (5,5′,6,6′-tetrachloro-1,1′,3,3′-tetraethyl-benzimidazolylcarbocyanide iodide) fluorescence (MMP, Figure 1B). This was further associated with increased transcription of *UCP-2* (Supplementary Figure S1G), which codes for the main uncoupling protein in human fibroblasts. The proton leak-dependent (oligomycin resistant) oxygen uptake increased about two-fold after IR-mediated arrest, similar to deep replicative senescence (Figure 1C), confirming mitochondrial uncoupling as an early event after DDR. Loss of MMP under DDR was also reflected by a diminished ability to maintain cellular $[Ca^{2+}]_i$ homeostasis (Supplementary Figure S2).

To see whether ROS production would also be induced in telomere-dependent senescence, we conditionally overexpressed a dominant-negative version of the telomere-binding protein TRF2 (TRF2$^{\Delta B\Delta M}$) by doxycycline removal (Supplementary Figures S3A–C). This induced purely telomere-dependent senescence (van Steensel *et al*, 1998) and resulted in comparable kinetics of appearance of mitochondrial dysfunction and ROS production as well as loss of growth potential and induction of DNA damage foci containing activated H2AX (γH2AX, Figure 1D and E; Supplementary Figures S3D–G). Antioxidant treatment (growth of cells under low ambient oxygen and under treatment with the free radical scavenger PBN) reduced, but did not abolish DNA damage foci induction (Supplementary Figure S3H). Retroviral transduction of TRF2$^{\Delta B\Delta M}$ into primary human MRC5 fibroblasts also induced a similar response (Supplementary Figure S4). Decreased MMP coupled with increased ROS levels is a hallmark of mitochondrial dysfunction that has recently been observed in senescent cells (Passos *et al*, 2007a). Our data now show that mitochondrial dysfunction is a delayed result of DDR regardless of how this is caused. We reasoned that such elevated ROS production might in turn contribute to DNA damage and DDR, thus forming a positive feedback loop.

Identification of a signalling pathway that induces ROS production and maintains DDR as part of a positive feedback loop
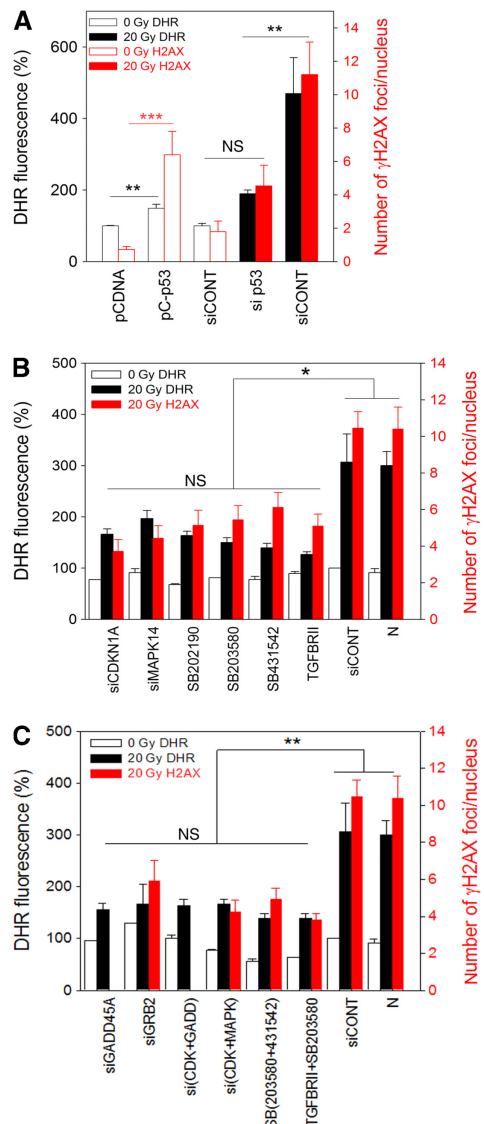
To test this idea and to delineate the signalling pathway between DDR and mitochondrial dysfunction/ROS

Figure 1 Mitochondrial dysfunction and ROS production are consequences of senescence. (**A**) MitoSOX, DHR and NAO fluorescence in irradiated MRC5 human fibroblasts at the indicated times after irradiation as measured by flow cytometry ($M \pm$ s.e.m., $n=3$). Asterisks indicate significant differences to non-irradiated controls (ANOVA). (**B**) Representative JC-1 confocal fluorescence images of MRC5 cells (red fluorescence indicates high MMP, green indicates low MMP, bar: 25 μm) and quantification of JC-1 ratios ($M \pm$ s.e.m., $n=3$). Differences are significant with $P<0.001$ (Mann–Whitney rank sum test). (**C**) Oligomycin-resistant (mitochondrial proton leak) respiration as proportion of basal (grey bars) and maximum (FCCP-) stimulated (black bars) mitochondrial oxygen uptake in young proliferating (YOUNG), deep senescent (SEN) and irradiated (IR) cells ($M \pm$ s.e.m., $n=9$–12). IR and SEN are different from YOUNG with $P<0.05$, but not from each other (ANOVA). (**D, E**) Doxocycline removal for 8 days (−DOX) in TRF2$^{\Delta B\Delta M}$ cells increased MitoSOX fluorescence (D) and decreased JC1 red/green ratio (E). Bar: 20 μm. Micrographs are representative for three experiments.

production, we first modulated *TP53* levels in MRC5 human fibroblasts and measured both ROS levels and DNA damage foci frequencies. TP53 overexpression increased cellular ROS levels and DNA damage foci frequencies, whereas siRNA-mediated knockdown of *TP53* before irradiation (Supplementary Figure S5) decreased both the parameters (Figure 2A). Inhibition of *CDKN1A, MAPK14* (by siRNA or small molecule inhibitors, Supplementary Figure S6) and TGFβ (by small molecule inhibitor or blocking antibody against TGFBRII) equally reduced ROS and DDR (Figure 2B), showing that the induction of mitochondrial dysfunction and ROS in senescent fibroblasts is not because of a direct interaction of TP53 with the mitochondria, but mediated through CDKN1A and MAPK14/TGFβ. This is in accordance with recent data showing that TP53 is not necessary for the DDR-dependent induction of senescence-associated interleukine secretion in fibroblasts (Rodier *et al*, 2009). There is also published evidence that TGFβ and p38 (MAPK14) activation can induce cellular ROS production through mitochondrial and non-mitochondrial (NADPHoxidase-dependent) pathways (Torres and Forman, 2003; Koli *et al*, 2008). Both have repeatedly been associated with induction of the senescent phenotype (Davis *et al*, 2005; Debacq-Chainiaux *et al*, 2005; Chretien *et al*, 2008) including DNA damage foci formation (Satyanarayana *et al*, 2004). However, the signalling hierarchy between TGFβ and MAPK14 with respect to mitochondrial ROS production and the connections, if any, to CDKN1A was not obvious.
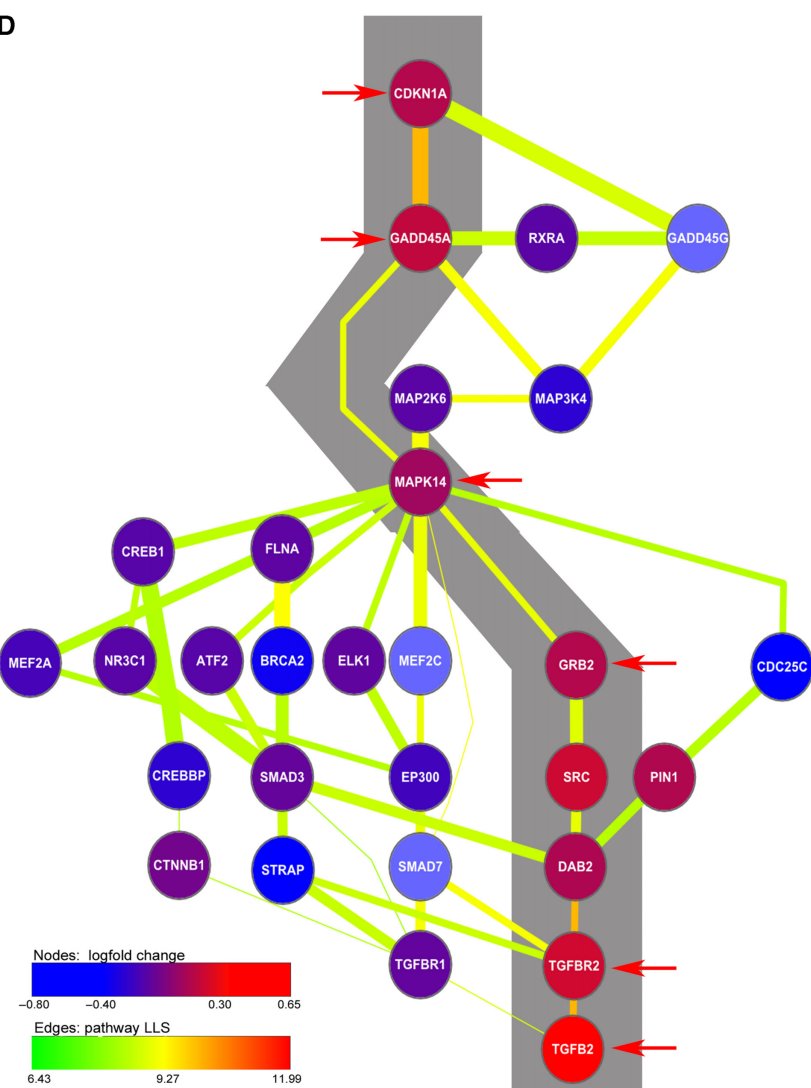
Figure 2 Feedback signalling through TP53-CDKN1A-GADD45A-MAPK14-GRB2-TGFBRII-TGFβ induces ROS production and maintains DDR. (**A–C**) MRC5 cells were transfected with wtTP53 (pC-p53), empty vector (pCDNA), siRNA as indicated, inhibitor treated or untreated (N). DHR fluorescence intensity (black) and γH2AX foci frequency (red) were measured in unirradiated cells and at 48 h after 20 Gy IR ($M \pm$ s.e.m., $n=3$). $^*P<0.04$, $^{**}P<0.01$, $^{***}P<0.001$ (ANOVA/Tukey), NS, not significant. (**D**) Pathways connecting CDKN1A to TGFβ through MAPK14. Edge thickness: LLS for any individual interaction; edge colour: pathway LLS; node colour: log fold mRNA change in senescent versus young MRC5; arrows: genes blocked in (B) and (C); grey: most probable pathway.

To identify candidate pathways connecting CDKN1A and either MAPK14 or TGFβ, we performed an *in-silico* interactome analysis. We first searched an interactome database combining Biogrid (Stark *et al*, 2006) and Phospho.ELM, a protein kinase target database (Diella *et al*, 2008) for all known paths between CDKN1A and either MAPK14 or TGFβ1/2 having not more than four intermediary nodes. We calculated the log likelihood score (LLS) of each pathway as the average of the LLS for each individual interaction involved. The 20 most probable pathways are shown in Supplementary Figure S7. Note that many of the interactions in Biogrid do not have an inherent directionality, so the resulting network is undirected. Path analysis therefore identified a number of false positive candidate pathways. However, all of the most probable pathways revealed a central position for the CDKN1A target

gene GADD45A (Supplementary Figure S7). GADD45A binds directly to CDKN1A (Kearsey *et al*, 1995) and can activate MAPK14 both indirectly (through MAP3K4 and MAP2K3) and directly (Bulavin *et al*, 2003).

To analyse experimentally the role of GADD45A and the hierarchy of MAPK14 and TGFβ, we performed further sequential candidate inhibitions, both singly and in various combinations. All treatments reduced ROS formation and DDR by a similar amount, and there was no additive effect for any of the combined treatments (Figure 2C), strongly suggesting that all tested gene products are members of one single epistatic pathway. Calculation of LLS in alternative pathways suggested that the probability for MAPK14 being upstream of TGFβ is about two orders of magnitude higher than for its being downstream (Supplementary Table S1). The most probable

pathway according to the interactome analysis is shown in Figure 2D. Overlaying the genes in these pathways with the results of an Affymetrix gene expression analysis of MRC5 fibroblast senescence (Passos *et al*, 2007a), we noted that the central genes in this pathway tend to be co-ordinately upregulated in senescent human fibroblasts, resulting in a tight cluster when subjected to unsupervised hierarchical clustering (Supplementary Figure S8). We further confirmed signalling through CDKN1A-MAPK14-TGFβ as part of a positive feedback loop combining DDR and ROS production by showing that (i) inhibition of MAPK14 reduced the amount of secreted TGFβ (Supplementary Figure S9A), increased MMP and decreased mitochondrial mass after IR (Supplementary Figure S9B); (ii) inhibition of either MAPK14 or TGFβ or both reduced DNA damage foci containing activated ATM/ATR and 53BP1 (Supplementary Figure S10); (iii) treatment with the MAPK14 inhibitor SB203580 lowered the levels of activated TP53 (p53-S15), CDKN1A and phosphorylated MAPK14 itself (Supplementary Figure S11); (iv) inhibition of MAPK14, but not of arachidonic acid metabolism, cytochrome P450 or PI3K signalling, specifically diminished the rise in ROS levels in telomere-dependent senescence (Supplementary Figure S12); (v) inhibition of MAPK14 and TGFβ, alone or in combination, reduced nuclear CDKN1A levels in MRC5 fibroblasts after IR (Supplementary Figure S13A); and (vi) scavenging of ROS reduced DDR foci frequencies and CDKN1A induction after IR (Supplementary Figure S13B).

Together, these data strongly suggested that the DDR and ultimately growth arrest in senescent cells might be maintained by a positive feedback loop between DDR and mitochondrial dysfunction/ROS production through signalling through TP53-CDKN1A-GADD45A-MAPK14-GRB2-TGFBRII-TGFβ (Supplementary Figure 3A).

A stochastic feedback loop model predicts the kinetics of DDR and growth arrest at the single cell level

We quantified the conceptual model shown in Figure 3A to see whether it could sufficiently explain the kinetics of senescence induction and maintenance. To create a stochastic mechanistic model of the DDR feedback loop, we extended our previously published model of the TP53/Mdm2 circuit (Proctor and Gray, 2008) to include reactions for synthesis/activation and degradation/deactivation/repair of CDKN1A, GADD45, MAPK14, ROS and DNA damage (Supplementary Tables S2 and S3). We chose realistic values for reaction rate constants and the initial amounts of the variables (see Supplementary Tables S2 and S3) and ran stochastic simulations for 500 cells initially from 2 days before until 6 days after IR. We parameterized the model using experimental kinetic data for TP53-S15, CDKN1A and MAPK14 protein levels (Supplementary Figure S11), DNA damage foci frequencies (Supplementary Figure S1E) and ROS levels (Figures 1A and 4A). The model replicated very precisely the kinetic behaviour of activated TP53, CDKN1A, ROS and DNA damage foci after irradiation. In simulations, the key variables stabilized after 2–3 days such that CDKN1A levels were maintained sufficiently above background to generate a stable growth arrest pheno-

type (Figure 3B). In contrast, a model without feedback would always return in less than 2–3 days to pre-irradiation levels (Figure 3C).
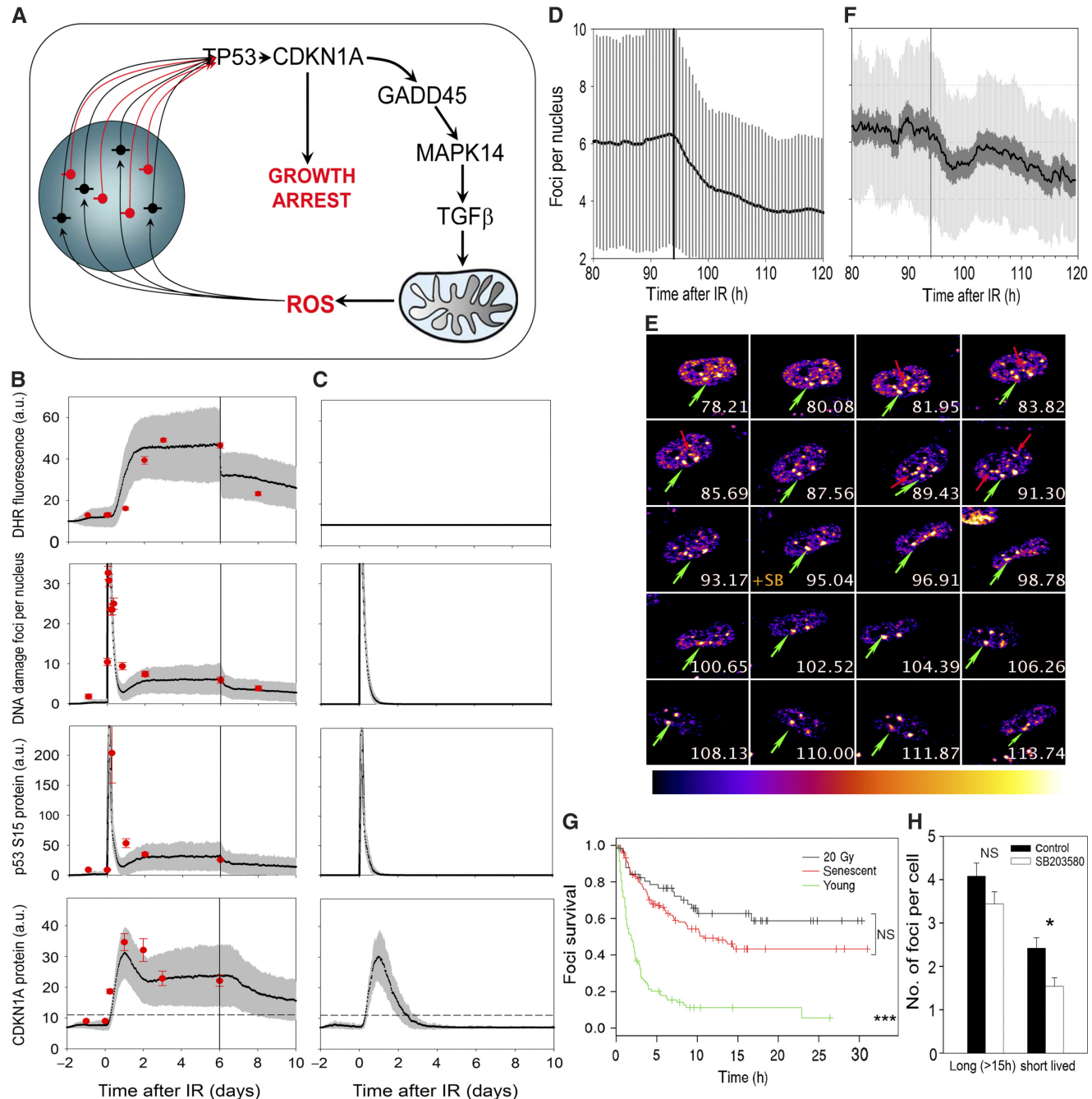
Having established its concordance with the experimental data, the model was then used to predict the effects of intervening in the feedback loop. Suppression of MAPK14 signalling or antioxidant treatment at day 6 after IR reduced ROS levels by about half (Figure 3B). The model predicted significantly decreased DDR and, importantly, reduced CDKN1A levels to an extent that would allow a fraction of cells to escape from growth arrest (Figure 3B). Thus, the model predicts that a feedback loop is both necessary and sufficient for the stability of growth arrest after induction of senescence by DNA damage.
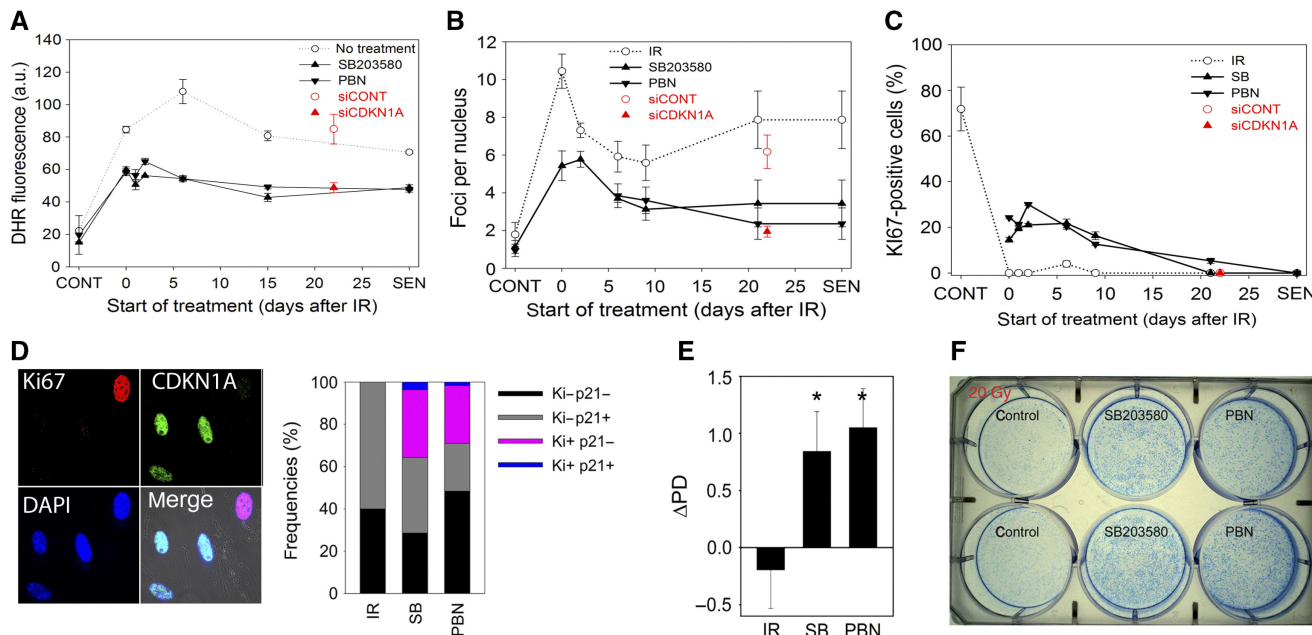
At higher time resolution, the model predicted a significant decline in DDR foci frequencies in IR-arrested cells within a few hours after MAPK14 inhibition (Figure 3D). To test this prediction, we used a 53BP1–GFP fusion protein as DDR reporter in live cells. 53BP1 is ubiquitously expressed and homogeneously distributed throughout the nucleus, and redistributes into foci after DNA damage. We fused a large C-terminal fragment of 53BP1, containing both the TUDOR and BRCT domains necessary for focus formation and interaction with TP53, to GFP, producing an AcGFP–53BP1c fusion protein that quantitatively reported foci dynamics in live cells (Nelson *et al*, 2009). DNA damage foci frequencies and levels of activated p53, CDKN1A and ROS all stabilized at around 2 days after IR and remained so over the following days (Figures 3B and 4A, B; Supplementary Figure S1E). Therefore, we visualized individual MRC5 fibroblasts stably expressing AcGFP–53BP1c from 3 day till up to 5 day after IR-mediated arrest. While under observation, the cells were treated with the MAPK14 inhibitor SB203580 at 94 h. Time-resolved live cell microscopy allowed the qualitative and quantitative identification of individual DNA damage foci (Figure 3E and Supplementary Movie SM1). Foci frequency measurements were in good agreement with static measurements by immunofluorescence (Supplementary Figure S10B) and quantitatively confirmed the prediction from the stochastic model (compare Figure 3D and F).

Closer observation of the time series revealed that the lifespan of many individual foci was much shorter than the observation period (see Supplementary Movie SM1). We ensured proper tracking of individual foci by using a wide z-stack range (4.5 μm) and a high imaging frequency (every 7 min). Appearance or disappearance, respectively, of foci on at least two consecutive images was used as recording criterion.

We measured the lifespan of individual foci in young proliferating, irradiated and deep senescent MRC5 fibroblasts (Figure 3G). There were few foci in proliferating cells, most of them with lifespans below 5 h, probably caused by replication stress. Foci lifespan increased significantly in senescent cells. However, even in deep telomere-dependent replicative senescence not all foci became permanent. Rather, about half of all foci were short lived with lifespans below 15 h (Figure 3G). Foci kinetics at >2 day after IR was very similar to that in replicative senescence (Figure 3G). Individual cell traces revealed that the reduction of total foci frequencies under SB203580 treatment was preferentially because of lower

Figure 3 A stochastic feedback loop model predicts the kinetics of DDR and growth arrest at the single cell level. (**A**) Feedback loop model. Uncapped telomeres (red) or unrepaired double strand breaks (black) trigger a DDR activating TP53 and CDKN1A. High CDKN1A levels initiate signalling through GADD45, MAPK14 and TGFβ leading to mitochondrial dysfunction and increased production of ROS, which damage nuclear DNA, thus inducing more non-telomeric DNA damage foci, stabilizing DDR and growth arrest leading to a stable senescent phenotype. (**B**) Stochastic simulations. IR at $t=0$, SB203580 from $t=6$ days. Results are $M \pm$ s.d., $n=500$. The vertical line indicates start of SB203580 treatment (inhibition of MAPK14 activity to 60%, compare Supplementary Figure S11). For CDKN1A, a threshold value at 2 s.d. above basal is indicated (dashed line). Experimental data (DHR flow cytometry for ROS, γH2A.X immunofluorescence for foci frequencies, CDKN1A/TUBULIN and p53 S15/total TP53 western, $M \pm$ s.e.m., $n \geqslant 3$) are shown in red for comparison. (**C**) The same simulation as in Figure 3B but completely without feedback after CDKN1A. (**D**) Effect of SB203580 treatment at 94 h after IR on DNA damage foci frequencies per cell as predicted by the stochastic model. M (black), s.d. (grey), $n=500$. (**E**) Confocal time series of an MRC5 cell expressing AcGFP–53BP1c at the indicated times (in h) after 20 Gy IR. SB203580 was added at $t=94$ h (+ SB). Images are compressed stacks (maximum intensity projections), focal depth=4.5 μm, with grey values converted to a colour scale as indicated in the lookup table. Full resolution time series is given in Supplementary Movie SM1. Green arrows indicate the one focus that is persistent over the whole observation period in this cell. All other foci are transient, and red arrows mark examples of these. (**F**) Frequencies of AcGFP–53BP1c foci after IR and under SB203580 treatment as measured by live cell microscopy. M (black), s.e.m. (dark), s.d. (light), $n=22$. The vertical bar indicates the start of treatment with SB203580 at $t=94$ h. (**G**) Kaplan–Mayer survival curves for AcGFP–53BP1c foci in young, senescent and irradiated MRC5 cells. Numbers of foci analysed are between 61 and 146 per treatment from two independent experiments. ***$P=1.1 \times 10^{-12}$ (Cox regression). (**H**) Frequencies of long- and short-lived AcGFP–53BP1c foci per cell (all irradiated with 20 Gy) before (control) and after start of treatment with SB203580. $M \pm$ s.e.m., $n=275-354$. *$P=0.006$; NS, not significant (Students' *t*-test).

**Figure 4** Feedback loop signalling is necessary and sufficient to maintain proliferation arrest during establishment of irreversible cell senescence. (**A**) ROS levels (DHR fluorescence intensity) in cells at the indicated times after 20 Gy IR and in young (CONT) and replicatively senescent (SEN) cells ($M \pm$ s.e.m., $n=3$). Treatments with either SB203580, PBN or siRNA against CDKN1A were started at the indicated times and ROS levels were measured at 48–72 h later. At all timepoints except CONT, $P < 0.01$ (ANOVA) for comparisons to IR-only treated cells. (**B**) Same experiment as in (A) with DNA damage foci frequencies measured. At all timepoints except CONT, $P < 0.01$ (ANOVA) for comparisons to IR-only treated cells. (**C**) Same experiment as in (A) with frequencies of KI67-positive cells measured. At all timepoints except CONT and >20d, $P < 0.01$ (ANOVA) for comparisons to IR-only treated cells. (**D**) MRC5 cells were irradiated, treated at day 6 with SB203580 or PBN and co-stained for Ki67 (red) and CDKN1A (green). Quantification of frequencies of unstained, single- and double-stained cells is on the right. (**E**) MRC5 cells in bulk culture were irradiated with 20 Gy, left untreated or treated with SB203580 or PBN at day 6 and cell numbers were counted at day 9 to calculate ΔPD ($M \pm$ s.e.m., $n=3$). PD did not change significantly in control, but increased under both treatments over controls with $P < 0.01$ (ANOVA). (**F**) Irradiated cells were plated at day 1 with 1000 cells/well and were left untreated or treated on day 6 with either SB203580 or PBN. Cells were stained on day 21.

numbers of short-lived foci (Supplementary Figure S14). Using a lifespan of 15 h as cut-off, we found a significant decrease in the frequency of short-lived, but not long-lived foci as a result of SB203580 treatment (Figure 3H). These data show that ROS production, mediated by a delayed signalling through MAPK14, contributes to DDR by constant replenishment of short-lived DNA damage foci.

The feedback loop between DDR and ROS production is necessary and sufficient to maintain senescent growth arrest during establishment of irreversible senescence

To analyse the relevance of the feedback loop for establishment and maintenance of the senescent phenotype we inhibited signalling through the loop at different time points after induction of SIPS by IR and measured ROS levels, DNA damage foci frequencies and proliferation markers. Treatments with the MAPK14 inhibitor SB203580 or the free radical scavenger PBN were used to block the loop, and a time frame from 30 min until 21 days after IR as well as deep replicative senescence was experimentally covered. Own (Supplementary Figure S1A) and published (Coppe *et al*, 2008; Rodier *et al*, 2009) data indicated that a full senescent phenotype develops over 7–10 days in human fibroblasts. Both treatments reduced ROS levels (Figure 4A) and γH2A.X foci frequencies

(Figure 4B) equally, even if started weeks after induction of senescence, indicating that the feedback loop remains active in deep senescence. Treatments also enhanced MMP over the whole time frame (data not shown). Treatments that were begun within 1 week after induction of DDR effectively rescued growth arrest (Figure 4C–F). After 20 Gy IR, all fibroblasts were stably negative for the proliferation-associated antigen Ki67, but this was rescued in up to 30% of the cells by treatment with either SB203580 or PBN, if the treatment was started within up to 9 days after induction of SIPS (Figure 4C). Almost all of the Ki67-positive cells were negative for expression of CDKN1A (Figure 4D), indicating that these cells were not merely re-entering G1 but had the potential to progress into the cell cycle. In fact, we observed robust recovery of proliferation in cells treated with SB203580 or PBN at 6 days after SIPS induction in both bulk culture (Figure 4E) and clonal growth (Figure 4F) assays. Treated cells grew at normal proliferation rates for at least several weeks whereas there was no growth at all in untreated cells after 20 Gy IR, indicating that the treatments not simply postponed but actually rescued senescence. Very similar results were obtained if cells irradiated with a lower dose of 5 Gy were treated either at 2 h (Supplementary Figure S15) or at 6 days after irradiation (Supplementary Figure S16). Moreover, post treatment of 5 Gy-irradiated cells with another antioxidant, *N*-acetylcysteine, rescued cell proliferation (data not shown).

We compared the experimentally observed rescue of growth with the predictions from the stochastic model. After single cell traces in the model, we observed that under SB203580 treatment some cells would for some time display CDKN1A values below the basal mean CDKN1A protein level as established in proliferating cells before IR (Supplementary Figure S17). We set a threshold level for CDKN1A in our stochastic model at $2 \times$ standard deviation above basal (see Figure 3B) and assumed that cells would recover from growth arrest if CDKN1A levels would remain continuously below this threshold for at least 6 h (i.e. allowing for passage through the CDKN1A-dependent G1/S border). Querying 500 individual cell tracks we found 96 cells (19.2%) under SB203580 treatment fulfilling this criterion, whereas none did so after IR alone (Supplementary Figure S16). A comparison with the experimental data (Figure 4C–F) shows that this model quantitatively predicts rescue of growth arrest by feedback loop inhibition.

Together, these results indicate that the feedback loop between DDR and ROS production is necessary and sufficient to maintain cell cycle arrest for at least 1 week after initiation of SIPS. However, at time points later than 9 days after initiation of senescence, the inhibition of feedback signalling became progressively less efficient in rescuing the arrest (Figure 4C), indicating that additional mechanisms not accounted for in our model stabilize growth arrest in deep senescence. Stabilization of the growth arrest in deep senescence might be due partly to gross changes in chromatin organization (Narita *et al*, 2003). Levels of senescence-associated heterochromatin foci (SAHF) and HP-1γ foci, two markers for senescence-associated chromatin re-modelling, were low at 6 days after IR but increased over the following weeks in parallel with the irreversibility of growth arrest (Supplementary Figure S18). Treatments of cells with either SB203580 or PBN at a late time point (10 days after IR), which did not effectively rescue growth, also did not change SAHF-associated nuclear granularity (Supplementary Figure S18C).

## DNA damage signalling through CDKN1A results in increased ROS-mediated damage *in vivo*
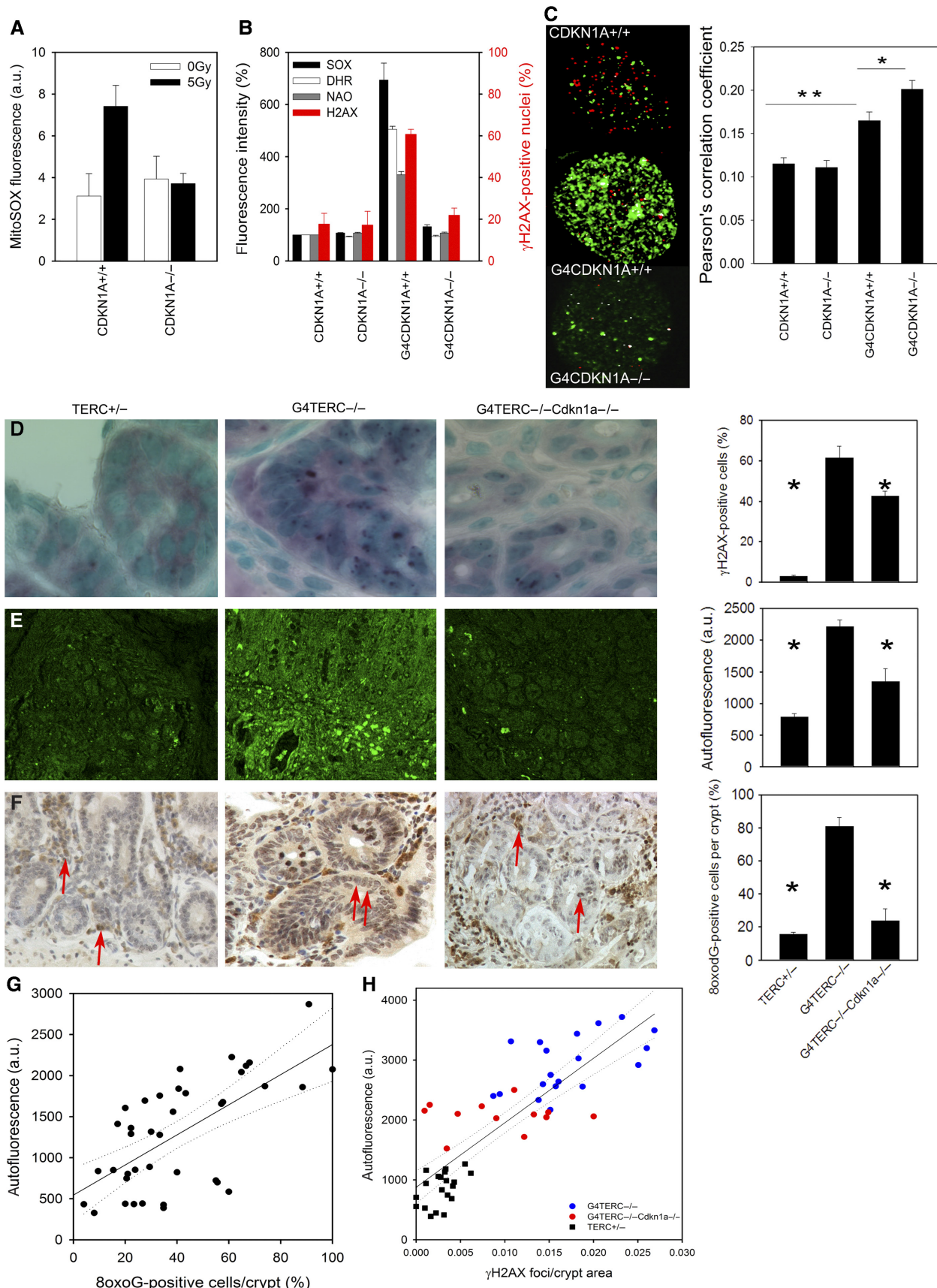
To assess the relevance of feedback loop signalling for generation of oxidative damage *in vivo* we used primary embryonic fibroblasts (mouse embryonic fibroblasts, MEFs) and tissues from late generation (G4) *TERC*−/− and *G4TERC*−/−*CDKN1A*−/− mice. Loss of telomerase function over multiple generations induces telomere dysfunction triggering widespread DDR in tissues. Knockout of *CDKN1A*

inhibited downstream signalling and partially rescued the shortened lifespan of *G4TERC*−/− mice (Choudhury *et al*, 2007). As in human cells, ROS levels increased in wt MEFs at 48 h after IR, and this was completely abolished in *CDKN1A*−/− MEFs (Figure 5A). Moreover, *CDKN1A* deletion suppressed the induction of ROS and DDR in telomere-dependent senescence (i.e. under low ambient oxygen) in *G4TERC*−/− MEFs (Figure 5B). Interestingly, the co-localization of telomeres and the remaining foci was closest in the double-KO MEFs, confirming that loss of signalling through CDKN1A preferentially reduced non-telomeric foci (Figure 5C). These data confirm the existence of a CDKN1A-dependent feedback loop signalling in mice cells very similar to that in human cells.

Frequencies of senescent cells displaying DNA damage foci increase with age in various cells and tissues of control mice including the enterocytes in intestinal crypts. We established that these foci-positive cells were not apoptotic and that very few of them were double positive for γH2A.X and proliferation markers (Wang *et al*, 2009). We obtained good quantitative agreement between estimates of Sen-β-Gal-positive and γH2A.X-positive, PCNA-negative enterocytes, strongly suggesting that these cells are senescent (Lawless *et al*, 2009). To assess whether this can contribute to an increased oxidative load *in vivo*, we measured γH2A.X foci formation together with two markers of tissue oxidative damage (broad-band autofluorescence and 8-oxodG immunoreactivity) in intestinal crypts from age-matched control, *G4TERC*−/− and *G4TERC*−/−*CDKN1A*−/− mice (Figure 5D–F). Frequencies of γH2A.X-positive enterocytes per crypt were significantly increased in *G4TERC*−/− as compared with wild type or *TERC*+/− mice (Figure 5D, see also (Choudhury *et al*, 2007; Wang *et al*, 2009)). Although loss of *CDKN1A* only mildly decreased the numbers of crypts showing any γH2A.X positivity (Choudhury *et al*, 2007), it significantly reduced the frequencies of γH2A.X-positive cells per crypt (Figure 5D and H). This effect was not related to apoptosis because frequencies of TUNEL-positive crypt cells were not dependent on *CDKN1A* (Choudhury *et al*, 2007).

Broad-band autofluorescence originates mainly from oxidized and cross-linked cell components, such as advanced glycation end products and the age pigment lipofuscin and is thus related to oxidative stress (Gerstbrein *et al*, 2005). Autofluorescence intensity was increased in crypts from *G4TERC*−/− mice, but this was rescued by loss of *CDKN1A* (Figure 5E). A similar pattern was seen for oxidative DNA base modification (Figure 5F). Autofluorescence was significantly correlated with 8-oxoG staining intensity (Figure 5G) and γH2A.X foci frequency on the single crypt level with only

Figure 5 *CDKN1A* knockout rescues oxidative damage in late generation *TERC*−/− mice. (**A**) MitoSOX fluorescence at 48 h after IR in MEFs. $M \pm$ s.e.m., $n=3$, $P=0.029$ (Student's *t*-test) for IR CDKN1A +/+ against IR CDKN1A−/−. (**B**) MitoSOX, DHR and NAO fluorescence intensities and frequencies of γH2AX-positive MEFs with the indicated genotypes. G4 indicates late generation *TERC*−/− $P<0.0001$ (ANOVA/Tukey) for *G4CDKN1A* +/+ against *G4CDKN1A*−/− (all parameters). (**C**) Representative micrographs of MEF nuclei. Red: telomeres; green: γH2A.X; white: significant co-localization according to a Pearson correlation analysis. Pearson correlation coefficients for telomere-foci colocalization in MEFs from the indicated genotypes on the right ($M \pm$ s.e.m., $n=80–90$, **$P<0.0001$, *$P=0.043$). MEFs in (A–C) were grown under 3% ambient oxygen concentration. (**D–F**) Representative micrographs of γH2A.X (D), broad-band autofluorescence (E) and 8oxodG immunostaining (F) in intestinal crypts from mice (aged 12–15 months) with the indicated genotypes. Quantitative data (right column) are $M \pm$ s.e.m., $n=3–5$. *$P<0.009$ against *G4TERC*−/− for all parameters (ANOVA/Tukey). Arrows in (F) show examples of 8oxodG-positive cells. (**G**) Frequencies of 8oxodG-positive cells versus autofluorescence in the same individual crypts. Linear regression (straight line) and 95% confidence intervals (dotted lines) are indicated. $P<0.0001$. (**H**) γH2A.X foci density versus autofluorescence in the same individual crypts from all three genotypes. Linear regression (straight line) and 95% confidence intervals (dotted lines) are shown.

© 2010 EMBO and Macmillan Publishers Limited

minor overlap between genotypes (Figure 5H). These data indicate that DNA damage signalling through CDKN1A contributes *in vivo* to oxidative damage in crypt cells.

CDKN1A-dependent ROS production is not restricted to proliferative tissues: Brain neurons suffer from intense DNA damage (Rass *et al*, 2007) and thus display frequent DNA damage foci (Sedelnikova *et al*, 2004). The frequency of cerebellar neurons showing a DDR increases in late generation *TERC*−/− mice, and this increase is partially rescued in *G4TERC*−/−*CDKN1A*−/− mice (Supplementary Figure S19A). Autofluorescence intensity and 8-oxodG positivity in these neurons changed in parallel (Supplementary Figures S19B–D). Similar data were obtained in the cortex and the hippocampus (not shown). These data show that telomere dysfunction induced oxidative damage *in vivo* through signalling through CDKN1A.

Discussion

The free radical hypothesis of aging regards ROS-mediated molecular damage as a potential cause of aging. Although there are conflicting results from intervention studies *in vivo* (Muller *et al*, 2007), an impact of ROS levels on senescence *in vitro* has been well documented (Passos *et al*, 2007b; Lu and Finkel, 2008). Our results show that mitochondrial dysfunction and ROS production can not only accelerate the onset of senescence (e.g. by accelerating telomere shortening, see (von Zglinicki, 2002)), but are also component and consequence of continuous DDR signalling and are thus an integral part of the senescent phenotype.

Takahashi *et al* (2006) were the first to convincingly show the existence of an ROS-generating positive feedback loop. In their model of human fibroblasts expressing a temperature-sensitive simian virus 40 large T antigen, the loop interconnected the CDKN2A pathway with ROS production and protein kinase C δ signalling (Takahashi *et al*, 2006). More recently, it was shown that oncogene-induced senescence can lead to AMPK activation, mitochondrial dysfunction and ROS production, which in turn can trigger senescence on its own (Moiseeva *et al*, 2009), so suggesting yet another feedback loop involving ROS in senescence. The retinoblastoma protein pRb is an important downstream mediator of growth arrest for both the CDKN1A and CDKN2A pathways (Chang *et al*, 2000; Dai and Enders, 2000; Beausejour *et al*, 2003; Takahashi *et al*, 2006). However, in our system of primary human or mouse fibroblasts neither CDKN2A nor pRb was necessarily involved in the induction of mitochondrial dysfunction and ROS production.

Although we do not rule out the existence of other pathways stabilizing ROS production in senescent cells, we have identified signalling through CDKN1A, MAPK14 and TGFβ as the important link between telomere-dependent and -independent DDR and ROS production in primary human and mice fibroblasts. This identification has been informed by *in silico* interactome analysis and quantitative stochastic modelling. Interactome analysis allows the integration of large amounts of data from a wide range of sources, even if they are available only in a dispersed set of databases, as is often the case with results of high-throughput experiments.

Possible relationships between genes that do not directly interact can be analysed by standard graph-theoretic algorithms, such as the shortest-paths analysis used here. The assignment of LLS to edges (Lee *et al*, 2004) provided a measure of strength to individual interactions, and permitted ranking of possible paths in order of biological plausibility. Major limitations of interactomes are their limited directionality and their static nature. As first steps to overcome these limitations, we combined Biogrid data with Phospho.ELM, a genome-wide protein phosphorylation database (Diella *et al*, 2008) and overlaid the results with a query-specific set of gene expression data.

A hallmark of aging processes, including cellular senescence, is their inherent stochastic heterogeneity (Kirkwood *et al*, 2005; Passos *et al*, 2007a). Therefore, we chose a quantitative model that can account for random processes and explain stochastic variation. This also enabled us to deal appropriately with molecular species present only at very low copy number (e.g. DNA damage foci) and with fractions of cells developing distinct outcomes (e.g. re-enter proliferation after intervention).

Importantly, we found that ROS levels increase in senescent cells as a result of signalling through CDKN1A-GADD45A-MAPK14-GRB2-TGFβ and feed back into DNA damage induction and response, generating a stable, self-sustaining feedback loop. This feedback loop persists even in irreversible deep senescence *in vitro* and in senescent cells *in vivo*. During the establishment phase of senescence, the loop is necessary and sufficient for maintenance of replication arrest. Thus, it is a necessary prerequisite for establishment of irreversible senescence.

Our data strongly suggest that during the early establishment phase of senescence a minimum frequency of DNA damage foci is necessary to maintain growth arrest long enough to allow cells to proceed towards irreversibility. This threshold frequency appears to be around five foci per nucleus in our experiments, but might be different in different cells and/or under different experimental conditions. Importantly, our data show that these foci do not have to be permanent themselves to induce permanent growth arrest. Cells might encounter permanent damage (i.e. uncapped telomeres) or high levels of, in principle, repairable damage (e.g. after high doses of IR). In any case, if this situation cannot be resolved within 1–2 days, a cell-autonomous program is activated, which permanently generates ROS and ROS-mediated DNA damage. The ensuing stochastic equilibrium of damage induction and repair maintains DNA damage signalling above threshold until further mechanisms (including but not necessarily limited to CDKN2A activation, autocrine signalling and chromatin remodelling) ensure permanent cell cycle arrest. Finding that about half of all foci in senescent cells are short lived, and that short-lived foci are necessary and sufficient to maintain stability of growth arrest in our model of SIPS does not imply that persistent, irreparable DNA damage signalling might not be sufficient to induce senescence under some conditions. However, it shows that the assumption that DNA damage needs to be irreparable and persistent to generate a persistent proliferation arrest is not necessary. Rather, transient DNA damage can have an important role for senescence, as long as it is constantly replenished by a positive

feedback loop that maintains a dynamic equilibrium between damage induction and repair.

An added layer of complexity is that foci composition can change with time. For instance, 53BP1, MRE11 and NBS1 are lost from DNA damage foci as cells enter mitosis, whereas γH2AX and MDC1 remain focally concentrated with chromatin (Nelson *et al*, 2009; Nakamura *et al*, 2010). Compositional changes of foci might also occur in tissues during aging (Panda *et al*, 2008). A better apprehension of foci dynamics will aid understanding of cellular damage responses and aging.

Oxygen levels in standard cell culture are unphysiologically high, and that causes increased ROS production at least partially from the mitochondria leading to acceleration of telomere-dependent senescence (von Zglinicki, 2002; Passos *et al*, 2007a) and/or SIPS (Parrinello *et al*, 2003). This does not imply that the induction of an ROS-generating feedback loop in senescence as described here is a cell culture artefact; however, ROS levels and DDR are still regulated in the same p21-dependent manner in MEFs under physiologically low ambient oxygen concentration (see Figure 5). Moreover, DDR and oxidative stress are closely associated during telomere-independent cell senescence in aging mice (Wang *et al*, 2009), and this association is dependent on p21 (this study). Telomere-dependent senescence can be postponed by lowering mitochondrial ROS production and/or release (Saretzki *et al*, 2003; Passos *et al*, 2007a), which might be due to both slower telomere shortening and decreased levels of non-telomeric DDR. Finally, recent data indicate that mitochondrial dysfunction and ROS production is triggered through p53- and pRb-dependent pathways in oncogenic ras-induced senescence and is able to contribute to ras-dependent growth arrest (Moiseeva *et al*, 2009). Together, these data suggest that a feedback loop involving mitochondrial dysfunction and ROS production might well be important in various physiologically relevant forms of cell senescence.

We speculate that mitochondrial dysfunction and ROS production might be causal for the development of the senescent phenotype. Mitochondrial dysfunction including ROS production induces retrograde response, a major reprogramming of nuclear gene expression patterns, in senescent cells (Butow and Avadhani, 2004; Passos *et al*, 2007a, c). Recent work implicated not only ROS (Bartek *et al*, 2007) but also factors involved in growth factor, chemokine and cytokine signalling as essential for oncogene-induced senescence (Acosta *et al*, 2008; Kuilman *et al*, 2008; Wajapeyee *et al*, 2008; Kuilman and Peeper, 2009). Many gene products from these families take part in retrograde response (Butow and Avadhani, 2004), and they interact with TP53 and MAPK pathways (Acosta *et al*, 2008). A detailed examination of the role of mitochondrial dysfunction for the establishment of the secretory senescent phenotype is clearly warranted.

Although senescent cells can be cleared away efficiently from tissues under some conditions (Ventura *et al*, 2007; Krizhanovsky *et al*, 2008), cells bearing various senescence markers including DNA damage foci do accumulate in human (Dimri *et al*, 1995), primate (Herbig *et al*, 2006) and mouse (Wang *et al*, 2009) tissues with advancing age. The fact that DNA damage foci are associated with ROS production *in vivo* and *in vitro* (this paper) suggests that tissue-resident cells with an activated DDR may disturb tissue function and homeostasis

not only by secreting biologically active peptides (Campisi and d'Adda di Fagagna, 2007; Coppe *et al*, 2008) but also by inducing ROS-mediated damage in their microenvironment. H_2O_2 is the main product of mitochondrial, cytoplasmic and extracellular superoxide dismutation. It is soluble in both water and lipid and is a relatively long-lived ROS, allowing for easy diffusion between cells. Thus, H_2O_2 release from cells with activated DDR might contribute to the 'bystander effect', whereby senescent cells appear to 'infect' their originally unstressed neighbours (Sokolov *et al*, 2007).

Importantly, our results show that interventions against individual components of the senescent phenotype (e.g. ROS production) are possible in deep senescence. Even if these interventions do not rescue the growth arrest phenotype, they can ameliorate the phenotypic impact of senescent cells onto their microenvironment (the 'bystander effect'). There is a preliminary evidence that 'anti-senescence' interventions have potential to delay aging. However, interventions upstream of the cell cycle checkpoint machinery may significantly increase cancer risk (Baker *et al*, 2008; Tomas-Loba *et al*, 2008). Improved understanding of the networks of signalling pathways that govern the senescent phenotype will undoubtedly help to identify the most promising targets to ameliorate the negative impact of aged cells on their environment.

Materials and methods

Cells and tissues

T19 cells containing a doxycycline inducible TRF2$^{\Delta B \Delta M}$ and the retroviral expression vector pLPCNMyc-TRF2 $^{\Delta B \Delta M}$ were gifts from T de Lange, Rockefeller University, NY (van Steensel *et al*, 1998). MRC-5 human embryonic lung fibroblasts (PD 38) were infected with pLPCNMyc-TRF2 $^{\Delta B \Delta M}$ retrovirus. Expression of TRF2$^{\Delta B \Delta M}$ was monitored using an anti-FLAG M2 mouse monoclonal antibody (Sigma) in T19 cells or the anti-Myc antibody Myc-FITC (#46-0307, Invitrogen) in infected MRC5. MEFs were grown under 3% ambient oxygen.

Transgenic mice were generated and MEFs as well as brain and gut sections from 12–15-months-old mice were prepared as described (Choudhury *et al*, 2007). Experiments were approved by the local ethics committee.

Inhibitors

MRC-5 cells at PD 25-30 were transiently transfected with either control untargeted siRNA, TP53 siRNA (SignalSilence® p53 siRNA kit, Cell Signalling Technology), CDKN1A siRNA (SignalSilence® p21 Waf1/Cip1 siRNA human specific), MAPK14 siRNA (SignalSilence® pool p38 MAPK siRNA) or GADD45A siRNA (GADD45A Validated Stealth™ DuoPak, Invitrogen) using nucleofection (Amaxa) according to the supplier's protocols.

MAPK14 activity was inhibited using 10 µM SB202190 (Sigma) or SB203580 (Tocris Bioscience). Inhibition was confirmed by western blot using anti-phospho-p38 MAPK (mouse monoclonal, Cell Signalling) and anti-p38 MAPK (rabbit polyclonal, Cell Signalling). Inhibition of the TGFβ pathway was performed using TGFβR2 antibody (rabbit polyclonal, Cell Signalling) or 10 µM SB431542 (Tocris Bioscience). Secreted human TGFβ1 was measured using Quantikine® Human TGF-β1 Immunoassay (#DB100B, R&D Systems).

Microscopy

Transmission electron microscopy was performed using conventional techniques. All fluorescence microscopy was performed in confocal

mode (Zeiss LSM510). Foci frequencies and fluorescence intensities were always measured under identical excitation and emission conditions using a $63 \times$ (NA=1.4) objective and a 1 Airy unit pinhole. For broad-band autofluorescence of $5 \mu m$ tissue sections a $20 \times$ (NA=0.5) objective with a pinhole equivalent to an $11 \mu m$ z-slice was used. The sample was excited at 458 nm and fluorescence emission captured above 475 nm, while simultaneously capturing a transmission image. Fluorescence intensities per cell or per crypt were quantified in ImageJ (http://rsb.info.nih.gov/ij/). MMP in live cells was measured by FACS (Passos *et al*, 2007a) or in a LSM510 equipped with a Solent incubator (Solent Scientific) at $37^{\circ}C$ with humidified 5% CO_2, using a $63 \times$ (NA=1.4) objective; 100 nM Mitotracker Green and 16 nM TMRM (tetramethylrhodamine methyl ester, Invitrogen) were loaded in serum-free medium for 30 min at $37^{\circ}C$. Mitotracker Green fluorescence (proportional to total mitochondrial mass) and TMRM fluorescence (proportional to MMP) were captured using 488 and 543 nm excitation and 505–530 nm bandpass or 560 nm longpass emission, respectively. Images of the entire cell depth were acquired using a $1.4 \mu m$ z-slice every 400 nm as z-stacks, deconvolved using Huygens (SVI) and rendered as surface projections using the same parameters for object size cut-off and intensity between different treatments.

To obtain quantitative estimates of SAHF formation, the mean gradient amplitude was calculated from DAPI-stained images in the masked region of interest and used as a measure of granularity using imageJ plugin http://bigwww.epfl.ch/thevenaz/differentials/ (Unser, 1999). Mean gradient amplitude was divided by mean DAPI intensity.

For live cell timelapse microscopy, cells were plated in Iwaki glass bottomed dishes (Iwaki) and imaged on an inverted Zeiss LSM510 equipped with a Solent incubator (Solent Scientific) at $37^{\circ}C$ with humidified 5% CO_2, using a 40×1.3 NA oil objective, as described (Nelson *et al*, 2002). Autofocus was performed at each timepoint before capturing a z-stack to ensure the entire cell was captured ($1.65 \mu m$ pinhole every $1.5 \mu m$ over $4.5 \mu m$ total z range). Cells and AcGFP–53BP1c foci were tracked manually using ImageJ (http://rsb.info.nih.gov/ij/).

Bioinformatics and quantitative stochastic modelling

A probabilistic functional integrated network of interactions was constructed using gene and protein interaction data from the BioGrid database (Stark *et al*, 2006), plus protein phosphorylation data from Phospho.ELM (Diella *et al*, 2008). To assess interaction likelihoods, an LLS was calculated for each dataset as described (Lee *et al*, 2004). Datasets larger than 100 interactions were analysed individually, whereas those with fewer than 100 interactions were grouped by evidence category. Pathway data, from the Kyoto Encyclopedia of Genes and Genomes (KEGG) (Kanehisa and Goto, 2000) Release 46.0, 1 April 2008, was used as the gold standard. The final LLS for an interaction between a pair of genes was calculated as the sum over the LLS of all the datasets containing that interaction.

Network analysis was performed using the Cytoscape platform (Shannon *et al*, 2003). An in-house Python script was used to detect all paths between CDKN1A and either MAPK14 or TGFβ1/2 having no more than four intermediary nodes.

For cluster analysis of candidate pathway genes, raw MRC5 microarray data (Passos *et al*, 2007a) (four young confluent and five senescent cultures) were loaded into Bioconductor (http://www.bioconductor.org) and normalized using GCRMA method. Hierarchical cluster analysis was applied to the expression values relative to the mean of all arrays. The Pearson correlation was used as similarity measure and average linkage as cluster method.

To test whether the feedback loop between DDR and ROS production was necessary to explain the experimental data, we developed a stochastic mechanistic model of the DDR extending our previously published model of the TP53/Mdm2 circuit (Proctor and Gray, 2008) by the steps outlined in Figure 5A. Model variables, reactions, kinetic laws and parameter values are given in Supplementary Tables S2 and S3. The model is encoded in the Systems Biology Markup Language (Hucka *et al*, 2003). Simulations are run in the Biology of Ageing e-Science Integration and Simulation (BASIS) system (http://www.

basis.ncl.ac.uk; Kirkwood *et al*, 2003; Gillespie *et al*, 2006) using stochastic simulation based on the exact Gillespie algorithm (Gillespie, 1977). The model is available in the public space of the BASIS database (urn:basis:ncl:basis:6178) and is also obtainable from Biomodels (MODEL 5989624192), http://www.ebi.ac.uk/biomodels/ (Le Novere *et al*, 2006).

Further experimental procedures

Flow cytometric and confocal imaging techniques to measure mitochondrial superoxide, cell peroxides, mitochondrial mass, cytoplasmic calcium, γH2A.X. immunofluorescence, telomere immuno-FISH, RT–PCR and sen-β-Gal staining were described (Passos *et al*, 2007a). All flow cytometry was performed on at least 30 000 cells per measurement. Anti-p21 mouse monoclonal IgG (U2OS, Calbiochem Inc.), anti-p16 rabbit polyclonal IgG (C20, Santa Cruz Biotechnology Inc.), anti-p38 MAPK rabbit polyclonal (Cell signalling) were used for immunofluorescence, and anti-γ-H2A.X rabbit monoclonal (Cell Signalling) and mouse monoclonal 8-oxodG (Japan Institute, with mouse-on-mouse kit) were used for immunohistochemistry with vectastain ABC kit (PK-6101, Vector).

Cellular oxygen uptake was determined using high-resolution respirometry (Oxygraph-2K; Oroboros Instruments, Insbruck, Austria). The measurements were taken at $37^{\circ}C$. After the recording of the rate of steady-state basal oxygen uptake, the following chemicals were sequentially added: oligomycin (1 µg/ml), carbonyl cyanide p-(trifluoromethoxy) phenylhydrazone (FCCP, 3–4.5 µM, depending on cell state), rotenone (0.5 µM) and antimycin A (2.5 µM). Antimycin-resistant oxygen uptake was registered as non-mitochondrial oxygen uptake and subtracted from the raw data to calculate the mitochondrial oxygen uptake.

Statistics

Group means were compared by Mann–Whitney rank sum test, if data were not normally distributed. Multiple comparisons were performed by ANOVA followed by Tukey's test for comparison of individual subgroups. γH2A.X-telomere co-localization was tested by pixelwise Pearson correlation analysis as described (Passos *et al*, 2007a).

Supplementary information

Supplementary information is available at the *Molecular Systems Biology* website (http://www.nature.com/msb).

Conflict of interest

The authors declare that they have no conflict of interest.

References

Acosta JC, O'Loghlen A, Banito A, Guijarro MV, Augert A, Raguz S, Fumagalli M, Da Costa M, Brown C, Popov N, Takatsu Y, Melamed J, d'Adda di Fagagna F, Bernard D, Hernando E, Gil J (2008)

Chemokine signalling via the CXCR2 receptor reinforces senescence. *Cell* **133**: 1006–1018

Baker DJ, Perez-Terzic C, Jin F, Pitel K, Niederlaender NJ, Jeganathan K, Yamada S, Reyes S, Rowe L, Hiddinga HJ, Eberhardt NL, Terzic A, van Deursen JM (2008) Opposing roles for p16Ink4a and p19Arf in senescence and ageing caused by BubR1 insufficiency. *Nat Cell Biol* **10**: 825–836

Bartek J, Bartkova J, Lukas J (2007) DNA damage signalling guards against activated oncogenes and tumour progression. *Oncogene* **26**: 7773–7779

Beausejour C, Krtolica A, Galimi F, Narita M, Lowe SW, Yaswen P, Campisi J (2003) Reversal of human cellular senescence: roles of the p53 and p16 pathways. *EMBO J* **22**: 4212–4222

Bulavin DV, Kovalsky O, Hollander MC, Fornace AJ (2003) Loss of oncogenic H-ras-induced cell cycle arrest and p38 mitogen-activated protein kinase activation by disruption of Gadd45a. *Mol Cell Biol* **23**: 3859–3871

Butow RA, Avadhani NG (2004) Mitochondrial signaling: the retrograde response. *Mol Cell* **14**: 1–15

Campisi J, d'Adda di Fagagna F (2007) Cellular senescence: when bad things happen to good cells. *Nat Rev Mol Cell Biol* **8**: 729–740

Chang BD, Broude EV, Fang J, Kalinichenko TV, Abdryashitov R, Poole JC, Roninson IB (2000) p21Waf1/Cip1/Sdi1-induced growth arrest is associated with depletion of mitosis-control proteins and leads to abnormal mitosis and endoreduplication in recovering cells. *Oncogene* **19**: 2165–2170

Chen QM, Fischer A, Reagan JD, Yan LJ, Ames BN (1995) Oxidative DNA damage and senescence of human diploid fibroblast cells. *Proc Natl Acad Sci USA* **92**: 4337–4341

Choudhury AR, Ju Z, Djojosubroto MW, Schienke A, Lechel A, Schaetzlein S, Jiang H, Stepczynska A, Wang C, Buer J, Lee HW, von Zglinicki T, Ganser A, Schirrmacher P, Nakauchi H, Rudolph KL (2007) CDKN1a deletion improves stem cell function and lifespan of mice with dysfunctional telomeres without accelerating cancer formation. *Nat Genet* **39**: 99–105

Chretien A, Dierick JF, Delaive E, Larsen MR, Dieu M, Raes M, Deroanne CF, Roepstorff P, Toussaint O (2008) Role of TGFb1-independent changes in protein neosynthesis, p38MAPK and cdc42 in hydrogen peroxide-induced senescence-like morphogenesis. *Free Radic Biol Med* **44**: 1732–1751

Coppe JP, Patil CK, Rodier F, Sun Y, Munoz DP, Goldstein J, Nelson PS, Desprez PY, Campisi J (2008) Senescence-associated secretory phenotypes reveal cell-nonautonomous functions of oncogenic RAS and the p53 tumor suppressor. *PLoS Biol* **6**: e301

d'Adda di Fagagna F (2008) Living on the break: cellular senescence as a DNA damage response. *Nat Rev Cancer* **8**: 512–522

d'Adda di Fagagna F, Reaper PM, Clay-Farrace L, Fiegler H, Carr P, Von Zglinicki T, Saretzki G, Carter NP, Jackson SP (2003) A DNA damage checkpoint response in telomere-initiated senescence. *Nature* **426**: 194–198

Dai CY, Enders GH (2000) p16INK4a can initiate an autonomous senescence program. *Oncogene* **19**: 1613–1622

Davis T, Baird DM, Haughton M, Jones CJ, Kipling D (2005) Prevention of accelerated cell aging in Werner syndrome using a p38 mitogen-activated protein kinase inhibitor. *J Gerontol A Biol Sci Med Sci* **60**: 1386–1393

Debacq-Chainiaux F, Borlon C, Pascal T, Royer V, Eliaers F, Ninane N, Carrard G, Friguet B, de Longueville F, Boffe S, Remacle J, Toussaint O (2005) Repeated exposure of human skin fibroblasts to UVB at subcytotoxic levels triggers premature senescence through the TGFbeta-1 signalling pathway. *J Cell Sci* **118**: 734–758

Diella F, Gould CM, Chica C, Via A, Gibson TJ (2008) Phospho.ELM: a database of phosphorylation sites—update 2008. *Nucleic Acids Res* **36**: D240–D244

Dimri GP, Lee X, Basile G, Acosta M, Scott G, Roskelley C, Medrano EE, Linskens M, Rubelj I, Pereira-Smith O (1995) A biomarker that identifies senescent human cells in culture and in aging skin *in vivo*. *Proc Natl Acad Sci USA* **92**: 9363–9367

Gerstbrein B, Stamatas G, Kollias N, Driscoll M (2005) *In vivo* spectrofluorimetry reveals endogenous biomarkers that report healthspan and dietary restriction in Caenorhabditis elegans. *Aging Cell* **4**: 127–137

Gillespie CS, Wilkinson DJ, Proctor C, Shanley DP, Boys RJ, Kirkwood TBL (2006) Tools for the SBML community. *Bioinformatics* **22**: 628–629

Gillespie DT (1977) Exact stochastic simulation of coupled chemical reactions. *J Phys Chem* **31**: 2340–2361

Herbig U, Ferreira M, Condel L, Carey D, Sedivy J (2006) Cellular senescence in aging primates. *Science* **311**: 1257

Hucka M, Finney A, Sauro HM, Bolouri H, Doyle JC, Kitano H, Arkin AP, Bornstein BJ, Bray D, Cornish-Bowden A, Cuellar AA, Dronov S, Gilles ED, Ginkel M, Gor V, Goryanin II, Hedley WJ, Hodgman TC, Hofmeyr JH, Hunter PJ *et al* (2003) The systems biology markup language (SBML): a medium for representation and exchange of biochemical network models. *Bioinformatics* **19**: 524–531

Kanehisa M, Goto S (2000) KEGG: Kyoto enzyclopedia of genes and genomes. *Nucleic Acids Res* **28**: 27–30

Kearsey JM, Cates PJ, Prescott AR, Warbrick E, Hall PA (1995) Gadd45 is a nuclear cell cycle regulated protein which interacts with p21Cip1. *Oncogene* **11**: 11675–11683

Kirkwood TBL (2005) Understanding the odd science of aging. *Cell* **120**: 437–448

Kirkwood TBL (2008) A systematic look at an old problem. *Nature* **451**: 644–647

Kirkwood TB, Boys RJ, Gillespie CS, Proctor CJ, Shanley DP, Wilkinson DJ (2003) Towards an e-biology of ageing: integrating theory and data. *Nat Rev Mol Cell Biol* **4**: 243–249

Kirkwood TB, Feder M, Finch CE, Franceschi C, Globerson A, Klingenberg CP, LaMarco K, Omholt S, Westendorp RG (2005) What accounts for the wide variation in life span of genetically identical organisms reared in a constant environment? *Mech Ageing Dev* **126**: 439–443

Koli K, Myllarniemi M, Keski-Oja J, Kinnula VL (2008) Transforming growth factor-beta activation in the lung: focus on fibrosis and reactive oxygen species. *Antioxid Redox Signal* **10**: 333–342

Krishnamurthy J, RTorrice C, Ramsey MR, Kovalev GI, Al-Regaiey K, Su L, Sharpless NE (2004) Ink4a/Arf expression is a biomarker of aging. *J Clin Invest* **114**: 1299–1307

Krizhanovsky V, Yon M, Dickins RA, Hearn S, Simon J, Miething C, Yee H, Zender L, Lowe SW (2008) Senescence of activated stellate cells limits liver fibrosis. *Cell* **134**: 657–667

Kuilman T, Michaloglou C, Vredefeld LCW, Douma S, van Doorn R, Desmet CJ, Aarden LA, Mooi WJ, Peeper DS (2008) Oncogene-induced senescence relayed by an interleukin-dependent inflammatory network. *Cell* **133**: 1019–1031

Kuilman T, Peeper DS (2009) Senescence-messaging secretome: SMS-ing cellular stress. *Nat Rev Cancer* **9**: 81–94

Lawless C, Wang C, Jurk D, Merz A, Von Zglinicki T, Passos JF (2009) Quantitative assessment of markers for cell senescence. *Exp Gerontol* (in press)

Le Novere N, Bornstein BJ, Broicher A, Coutot M, Donizelli M, Dharuri H, Li L, Sauro HM, Schilstra M, Shapiro B, Snoep JL, Hucka M (2006) BioModels Database: a free, centralized database of curated, published, quantitative kinetic models of biochemical and cellular systems. *Nucleic Acids Res* **34**(Suppl 1): D689–D691

Lee I, Date SV, Adai AT, Marcotte EM (2004) A probabilistic functional network of yeast genes. *Science* **306**: 1555–1558

Lu T, Finkel T (2008) Free radicals and senescence. *Exp Cell Res* **314**: 1918–1922

Macip S, Igarashi M, Berggren P, Yu J, Lee SW, Aaronson SA (2003) Influence of induced reactive oxygen species in p53-mediated cell fate decisions. *Mol Cell Biol* **23**: 8576–8585

Macip S, Igarashi M, Fang L, Chen A, Pan ZQ, Lee SW, Aaronson SA (2002) Inhibition of p21-mediated ROS accumulation can rescue p21-induced senescence. *EMBO J* **21**: 2180–2188

Minamino T, Komuro I (2007) Vascular cell senescence: contribution to atherosclerosis. *Circ Res* **100:** 15–26

Moiseeva O, Bourdeau V, Roux A, Deschemes-Simard X, Ferbeyre G (2009) Mitochondrial dysfunction contributes to oncogene-induced senescence. *Mol Cell Biol* **29:** 4495–4507

Muller FL, Lustgarten MS, Jang Y, Richardson A, van Remmen H (2007) Trends in oxidative aging theories. *Free Radic Biol Med* **43:** 477–503

Nakamura A, Rao VA, Pommier Y, Bonner WM (2010) The complexity of phosphorylated H2AX foci formation and DNA repair assembly at DNA double strand breaks. *Cell Cycle* **9:** 389–397

Narita M, Nunez S, Heard E, Narita M, Lin AW, Hearn SA, Spector DL, Hannon GJ, Lowe SW (2003) Rb-mediated heterochromatin formation and silencing of E2F target genes during cellular senescence. *Cell* **113:** 703–716

Nelson G, Buhmann M, Von Zglinicki T (2009) DNA damage foci in mitosis are devoid of 53BP1. *Cell Cycle* **8:** 3379–3383

Nelson G, Paraoan L, Spiller DG, Wilde GJ, Browne MA, Djali PK, Unitt JF, Sullivan E, Floettmann E, White MR (2002) Multi-parameter analysis of the kinetics of NF-kappaB signalling and transcription in single living cells. *J Cell Sci* **115:** 1137–1148

Panda S, Isbatan A, Adami GR (2008) Modification of the ATM/ATR directed DNA damage response state with aging and long after hepatocyte senescence induction *in vivo*. *Mech Ageing Dev* **129:** 332–340

Parrinello S, Samper E, Krtolica A, Goldstein J, Melov S, Campisi J (2003) Oxygen sensitivity severely limits the replicative lifespan of murine fibroblasts. *Nat Cell Biol* **5:** 741–747

Passos J, Saretzki G, Ahmed S, Nelson G, Richter T, Peters H, Wappler I, Birkett M, Harold G, Schaeuble K, Birch-Machin M, Kirkwood TBL, von Zglinicki T (2007a) Mitochondrial dysfunction accounts for the stochastic heterogeneity in telomere-dependent senescence. *PLoS Biol* **5:** e110

Passos J, Saretzki G, Von Zglinicki T (2007b) DNA damage in telomeres and mitochondria during cellular senescence: is there a connection? *Nucleic Acids Res* **35:** 7505–7513

Passos J, von Zglinicki T, Kirkwood TBL (2007c) Mitochondria and ageing: winning and losing in the numbers game. *Bioessays* **29:** 908–917

Polyak K, Xia Y, Zweier JL, Kinzler KW, Vogelstein B (1997) A model for p53-induced apoptosis. *Nature* **389:** 300–305

Proctor C, Gray D (2008) Explaining oscillations and variability in the p53-Mdm2 system. *BMC Syst Biol* **2:** 75

Rai P, Onder TT, Young JJ, McFaline JL, Pang B, Dedon PC, Weinberg RA (2008) Continuous elimination of oxidized nucleotides is necessary to prevent rapid onset of cellular senescence. *Proc Natl Acad Sci USA* **106:** 169–174

Ramsey MR, Sharpless NE (2006) ROS as tumour suppressor? *Nat Cell Biol* **8:** 1213–1215

Rass U, Ahel I, West SC (2007) Defective DNA repair and neurodegenerative disease. *Cell* **130:** 991–1004

Rodier F, Coppe JP, Patil CK, Hoeijmakers WAM, Munoz DP, Raza SR, Freund A, Campeau E, Davalos AR, Campisi J (2009) Persistent DNA damage signalling triggers senescence-associated inflammatory cytokine secretion. *Nat Cell Biol* **11:** 973–979

Rudolph KL, Chang S, Lee HW, Blasco M, Gottlieb GJ, Greider C, DePinho RA (1999) Longevity, stress response, and cancer in aging telomerase-deficient mice. *Cell* **96:** 701–712

Sang L, Coller HA, Roberts JM (2008) Control of the reversibility of cellular quiescence by the transcriptional repressor HES1. *Science* **321:** 1095–1100

Saretzki G, Murphy MP, von Zglinicki T (2003) MitoQ counteracts telomere shortening and elongates lifespan of fibroblasts under mild oxidative stress. *Ageing Cell* **2:** 141–143

Satyanarayana A, Greenberg RA, Schaetzlein S, Buer J, Masutomi K, Hahn WC, Zimmermann S, Martens UM, Manns MP, Rudolph KL (2004) Mitogen stimulation cooperates with telomere shortening to activate DNA damage responses and senescence signaling. *Mol Cell Biol* **24:** 5459–5474

Sedelnikova OA, Horikawa I, Zimonjic DB, Popescu NC, Bonner WM, Barrett JC (2004) Senescing human cells and ageing mice accumulate DNA lesions with unrepairable double-strand breaks. *Nat Cell Biol* **6:** 168–170

Shannon P, Markiel A, Ozier O, Baglia NS, Wang JT, Ramage D, Amin N, Schwikowski B, Ideker T (2003) Cytoscape: a software environment for integrated models of biomolecular interaction networks. *Genome Res* **13:** 2498–2504

Shelton DN, Chang E, Whittier PS, Choi D, Funk WD (1999) Microarray analysis of replicative senescence. *Curr Biol* **9:** 939–945

Sokolov MV, Dickey JS, Bonner WM, Sedelnikova OA (2007) gamma-H2AX in bystander cells: not just a radiation-triggered event, a cellular response to stress mediated by intercellular communication. *Cell Cycle* **6:** 2210–2212

Sone H, Kagawa Y (2005) Pancreatic beta cell senescence contributes to the pathogenesis of type 2 diabetes in high-fat diet-induced diabetic mice. *Diabetologia* **48:** 58–67

Stark C, Breitkreutz BJ, Reguly T, Boucher L, Breitkreutz A, Tyers M (2006) BioGRID: a general repository for interaction datasets. *Nucleic Acids Res* **34:** D535–D539

Takahashi A, Ohtani N, Yamakoshi K, Iida S, Tahara H, Nakayama K, Nakayama KI, Ide T, Saya H, Hara E (2006) Mitogenic signalling and the p16INK4A-RB pathway cooperate to enforce irreversible cellular senescence. *Nat Cell Biol* **8:** 1291–1297

Tomas-Loba A, Flores I, Fernandez-Marcos PJ, Cayuela ML, Maraver A, Tejera AM, Borras C, Matheu A, Klatt P, Flores JM, Vina J, Serrano M, Blasco MA (2008) Telomerase reverse transcriptase delays aging in cancer-resistant mice. *Cell* **135:** 609–622

Torres M, Forman HJ (2003) Redox signalling and MAP kinase pathways. *Biofactors* **17:** 287–296

Tyner SD, Venkatachalam S, Chol J, Jones S, Ghebranious N, Igelmann H, Lu X, Soron G, Cooper B, Brayton C, Park SH, Thompson T, Karsenty G, Bradley A, Donehower LA (2002) p53 mutant mice that display early ageing-associated phenotypes. *Nature* **415:** 45–53

Unser M (1999) Splines: a perfect fit for signal and image processing. *IEEE Signal Process Mag* **16:** 22–38

van Steensel B, Smogorzewska A, de Lange T (1998) TRF2 protects human telomeres from end-to-end fusions. *Cell* **92:** 401–413

Ventura A, Kirsch DG, McLaughlin ME, Tuveson DA, Grimm J, Lintault L, Newman J, Reczek EE, Weissleder R, Jacks T (2007) Restoration of p53 function leads to tumour regression. *In vivo*. *Nature* **445:** 661–665

von Zglinicki T (2002) Oxidative stress shortens telomeres. *Trends Biochem Sci* **27:** 339–344

Wajapeyee N, Serra RW, Zhu X, Mahalingam M, Green MR (2008) Oncogenic BRAF induces senescence and apoptosis through pathways mediated by the secreted protein IGFBP7. *Cell* **132:** 363–374

Wang C, Jurk D, Maddick M, Nelson G, Martin-Ruiz C, Von Zglinicki T (2009) DNA damage response and cellular senescence in tissues of aging mice. *Aging Cell* **8:** 311–323